

1 High-frequency variability in the  
2 North Icelandic Jet

3 B. E. Harden<sup>1</sup> and R. S. Pickart

4 Woods Hole Oceanographic Institution, Woods Hole, USA

5 January 11, 2018

<sup>1</sup>Woods Hole Oceanographic Institution, 266 Woods Hole Road, Woods Hole, MA 02543.  
bharden@whoi.edu

**ABSTRACT**

7 We describe the high-frequency variability in the North Icelandic Jet on the Iceland Slope  
8 using data from the densely instrumented Kögur mooring array deployed upstream of the  
9 Denmark Strait sill from September 2011 to July 2012. Significant sub-8-day variability  
10 is ubiquitous in all moorings from the Iceland slope with a dominant period of 3.6 days.  
11 We attribute this variability to Topographic Rossby Waves on the Iceland slope with a  
12 wavelength of  $62 \pm 3$  km and a phase velocity of  $17.3 \pm 0.8$  km day<sup>-1</sup> directed downslope  
13 ( $-9^\circ\text{T}$ ). We test the theoretic dispersion relation for these waves against our observations  
14 and find good agreement between the direction of phase propagation. We additionally  
15 calculate a theoretical group velocity of  $36$  km day<sup>-1</sup> directed almost directly up-slope  
16 ( $138^\circ\text{T}$ ) which agrees well with the propagation speed and direction of observed energy  
17 pulses. We use a wave tracing model to show that this wave energy is generated locally,  
18 offshore of the array, and not in the upstream or downstream directions. We hypothesize  
19 that either the meandering Separated East Greenland Current at the foot of the Iceland  
20 slope or intermittent aspiration into the Denmark Strait Overflow are the drivers of the  
21 Topographic Rossby Waves. Regardless of the formation mechanism, the waves appear to  
22 be a local phenomena, not found in an instrumented record upstream.

## 23 1. Introduction

24 The Denmark Strait Overflow is the major pathway of dense water out of the Nordic  
25 Seas. It transports 3.2 Sv, or approximately 50%, of the total outflow (Dickson and Brown,  
26 1994; Jochumsen *et al.*, 2017), and hence plays a crucial role in the Atlantic meridional  
27 overturning circulation (AMOC). While the existence of this overflow has been known  
28 for many decades, our understanding of the processes that govern it and the underlying  
29 dynamics remains incomplete. One important aspect that requires further study is deter-  
30 mining the upstream sources of the dense water and how it approaches the sill. If we are to  
31 determine how a changing climate might impact the AMOC, we need to understand bet-  
32 ter the connection between the water mass transformation process and the flux of newly  
33 ventilated water to Denmark Strait.

34 Most of the Denmark Strait Overflow water (approximately 70%) comes from the  
35 East Greenland Current by way of the Nordic Seas boundary current system (Våge *et al.*,  
36 2013; Harden *et al.*, 2016) (see Figure 1). Specifically, warm Atlantic inflow across the  
37 Greenland-Scotland Ridge is progressively cooled as it flows northward towards Fram  
38 Strait, much of it recirculating in the strait and subducting to mid-depth (Mauritzen, 1996).  
39 This is joined by Atlantic water exiting the strait that has circumnavigated the Arctic, and  
40 together the transformed Atlantic water flows southward in the East Greenland Current. As  
41 the current rounds Scoresby Sund, it splits into two branches (Figure 1). One continues to-  
42 wards the sill as a shelfbreak jet (Håvik *et al.*, 2017). The other carries approximately 60%  
43 of the East Greenland Current water out into the central strait via eddies and/or gyre-like  
44 deflections of the shelfbreak jet (Våge *et al.*, 2013; Harden *et al.*, 2016). This separated  
45 pathway then flows into the strait along the outer Iceland slope.

46 The remaining 30% of Denmark Strait Overflow water is supplied by the North Ice-  
47 landic Jet (NIJ), a more recently discovered branch of the upstream circulation (Jonsson  
48 and Valdimarsson, 2004; Våge *et al.*, 2011). This mid-depth intensified jet advects waters  
49 distinct from those found in the East Greenland Current (colder and fresher) suggestive of

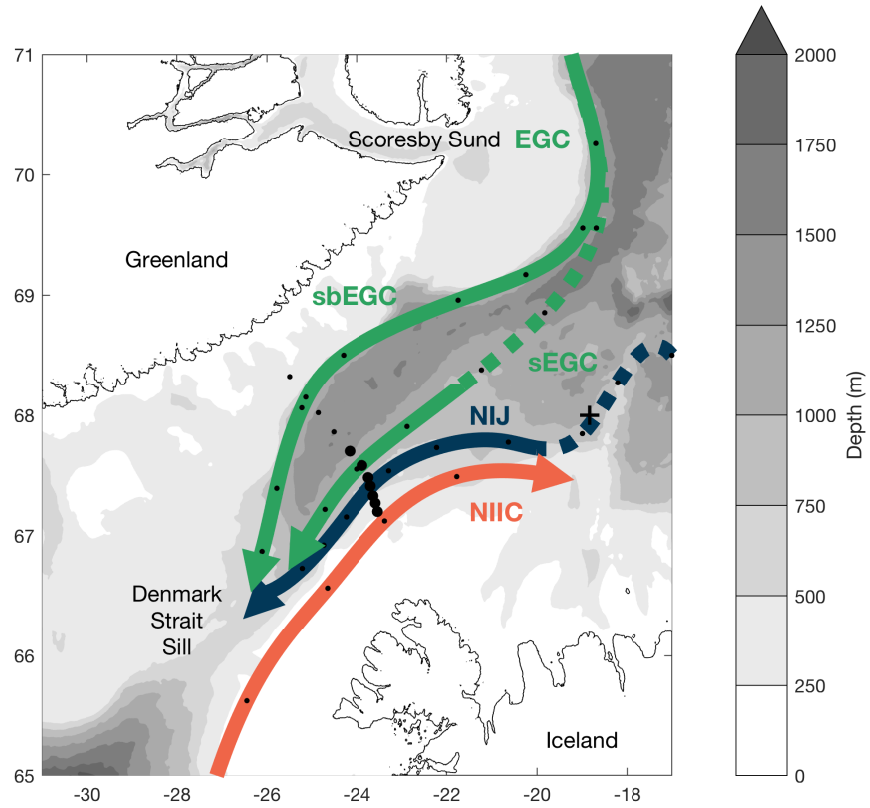


Figure 1: Map of the study region showing the overflow pathways approaching the Denmark Strait Sill: the North Icelandic Jet (NIJ) and the two East Greenland Current (EGC) pathways, one along the shelfbreak (sbEGC) and the other in a separated branch on the Iceland Slope (sEGC). Dashed portions show parts of pathways that still need further clarification. Also shown is the northward flowing surface-intensified current, the North Icelandic Irminger Current (NIIC). Black dots show the locations of the moorings in the Kögur array with larger dots indicating the subset of seven moorings used in this study. The upstream cross is the mooring to the west of the Kolbensey ridge referred to in the text. The bathymetry is from IBCAO v3.

50 a source in the central Iceland or Greenland seas (Våge *et al.*, 2011; 2015; Harden *et al.*,  
51 2016). The NIJ contains the densest water that feeds the overflow; its waters are found in  
52 the deepest part of the sill (Mastropole *et al.*, 2017) and subsequently sink to the deepest  
53 depths in the core of the overflow.

54 The leading hypothesis for the formation of the NIJ, supported by both models and  
55 observations, is that it represents the lower limb of a local overturning cell in the Iceland  
56 sea (Våge *et al.*, 2011; Behrens *et al.*, 2017). The upper limb of the cell is the NIIC, which  
57 sheds warm water into the Iceland Sea that is cooled by air-sea heat loss. The transformed  
58 water then returns southward towards the boundary where it sinks and forms the NIJ.  
59 However, many questions remain unanswered about this proposed system. For instance,  
60 the winter mixed-layers in the Iceland Sea don't appear to be dense enough to account for  
61 the deepest water in the NIJ (Våge *et al.*, 2015), whereas those in the Greenland Sea do  
62 (Strass *et al.*, 1993; Rudels *et al.*, 2002).

63 Regardless of the source of the NIJ, it clearly constitutes a vital component of the  
64 circulation upstream of the sill. Harden *et al.* (2016) investigated the jet's mean and sea-  
65 sonal contribution to the overflow, demonstrating that there is time-dependent partitioning  
66 of transport between the NIJ and the other two overflow branches on weekly to monthly  
67 timescales, likely driven by the wind. Pickart *et al.* (2017) noted that the NIJ appears to  
68 be coupled to the northward-flowing NIIC and that, on occasion, it consists of multiple  
69 branches. Using historical hydrographic data, Pickart *et al.* (2017) also revealed a clear  
70 link between the interannually varying properties of the NIJ and those of the densest water  
71 at the Denmark Strait sill, leaving little doubt that the NIJ is a major source of the overflow  
72 plume.

73 It has long been known that the Denmark Strait Overflow varies on short (order days)  
74 timescales (Smith, 1976; Bruce, 1995; Käse *et al.*, 2003). Some of this variability is as-  
75 sociated with the passage of lenses of cold, dense, overflow water referred to as boluses  
76 (Cooper, 1955). Recently, Appen *et al.* (2017) identified a second type of mesoscale fea-

77 ture in the strait that was termed a pulse. In contrast to boluses, pulses correspond to a  
78 thinning of the overflow layer associated with a large increase in equatorward velocity.  
79 Both of these features have been identified in a high-resolution regional model as well  
80 (Almansi *et al.*, 2017). Appen *et al.* (2017) showed that, between boluses and pulses, a  
81 mesoscale feature passes through Denmark Strait on average every 2 days. Presently, how-  
82 ever, it is unknown if these disturbances originate from upstream or if they are associated  
83 with local dynamics near the sill.

84 The goal of the present study is to shed light on some of the above processes by de-  
85 scribing the high frequency variability of the NIJ north of the Denmark Strait. We use  
86 timeseries data from a year-long mooring array that was maintained roughly 200 km up-  
87 stream of the sill (Figure 1). This is the same data set used by Harden *et al.* (2016) to  
88 investigate the mean and seasonal attributes of the NIJ. While Harden *et al.* (2016) men-  
89 tioned that the NIJ exhibits high-frequency variability, they did not elaborate. We begin  
90 with a brief description of the data, followed by a characterization of the high-frequency  
91 signal. We discuss how this signal is consistent with the existence of Topographic Rossby  
92 waves on the Iceland slope and go on to investigate the source region of the energy in these  
93 waves through inverse wave tracing.

## 94 **2. Data and Methods**

95 The data for this study come from the densely instrumented Kögur mooring array  
96 spanning the Denmark Strait approximately 200 km upstream of the sill. The array was  
97 deployed for 11 months from September 2011 to July 2012 and consisted of 12 moorings  
98 (named KGA 1-12) equipped with instrumentation to measure both the hydrography and  
99 velocity of the water column from 50 m to the bottom. Harden *et al.* (2016) present a  
100 detailed description of the mooring data, including the instrumentation, processing steps,  
101 and sensor accuracies. The array captured the majority of the overflow water (denser than  
102  $27.8 \text{ kg m}^{-3}$ ) passing through the northern part of the strait towards the sill.

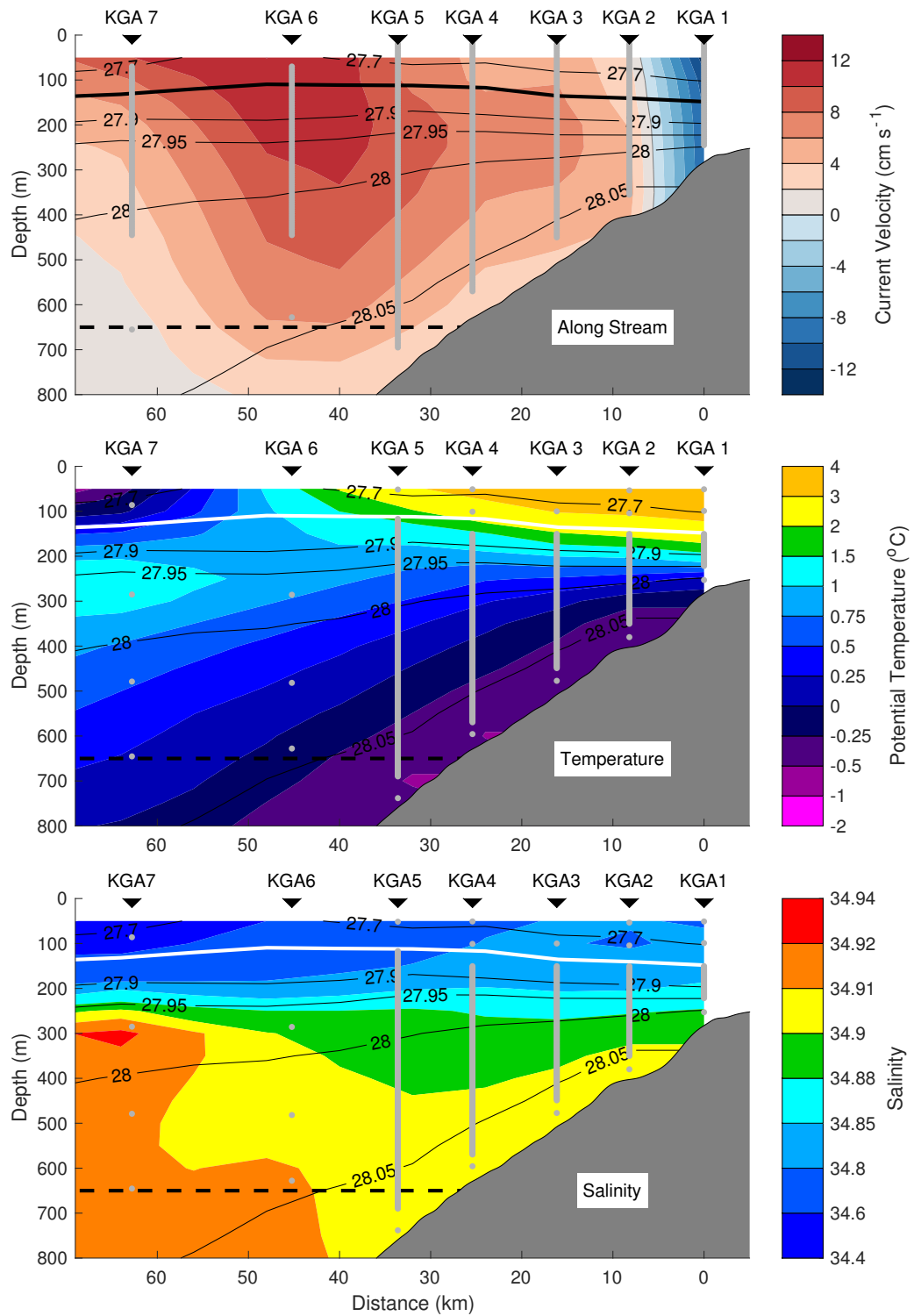


Figure 2: Mean vertical section of the along-stream (cross-transect) velocity (top), and median sections of potential temperature (middle) and salinity (bottom) for the 11-month period of the Kögur array. Overlaid in black contours on each panel is the mean density with the  $27.8 \text{ kg m}^{-3}$  isopycnal (the upper boundary of Denmark Strait Overflow Water) highlighted. The viewer is looking to the northeast with Iceland on the right. Positive velocities are equatorward. The horizontal black dashed line indicates the depth of the Denmark Strait sill. The moorings (black triangles) are labeled, and the average instrument locations are shown by the grey points. The bathymetry is from a shipboard echosounder.

103 Here we use primarily the gridded product described in Harden *et al.* (2016), which  
104 has a lateral resolution of 8km and vertical resolution of 50 m. Because of our focus  
105 on the Iceland slope, we consider a subset of these data up to and including the location  
106 of mooring KGA 7, approximately 70 km offshore of the Iceland shelfbreak. The mean  
107 velocity sections demonstrate that this portion of the array captures both the NIJ and the  
108 majority of the Separated EGC (Figure 2). For parts of the analysis we also use the data  
109 on a mooring-by-mooring basis. All of the velocities have been de-tided using a 36-hour  
110 low-pass filter.

111 Additional data come from a mooring located approximately 200 km upstream of the  
112 Kögur Array on the west side of the Kolbesney Ridge (68°00'N, 18°50'W, see Figure  
113 1) This was deployed on the 1000 m isobath from September 2007 to mid-October 2008  
114 and consisted of a McLane Moored Profiler and acoustic current meter providing profiles  
115 between 100 m and the bottom at 8 hour intervals. As with the Kögur data, we low-passed  
116 the velocity timeseries using a 36-hr filter to remove the tidal components of the flow.  
117 These data are described in greater detail by Jónsson and Valdimarsson (2012).

118 The inverse wave tracing of topographic Rossby waves (TRWs) was done using the  
119 model described by Meinen *et al.* (1993) and implemented by Pickart (1995) for investigat-  
120 ing TRWs in the Deep Western Boundary Current off of Cape Hatteras, North Carolina.  
121 The method uses the TRW dispersion relation to calculate the group velocity and then  
122 backtracks the evolution of the wave with a time step of 30 minutes. The wave parameters  
123 are recalculated at each step for the local bottom depth, bottom slope, and water column  
124 stratification. A new group velocity is then found and used to further trace the wave. Most  
125 of the required input parameters for the inverse wave tracing model come directly from the  
126 moored data and are the same as those used for the theoretical TRW dispersion relation  
127 calculations (see Section 3.a.). For the bathymetry we used the International Bathymetric  
128 Chart of the Arctic Ocean 30-arcsec gridded product (Jakobsson *et al.*, 2012). To remove  
129 seamounts and other sharp topographic features we smoothed the bathymetry using a filter



130 of 60 km (comparable to our measured TRW wavelength). In contrast to Pickart (1995)  
131 who subsequently fit splines to the data to be able to find the bottom depth and gradients  
132 at any location, we deemed our resolution to be high enough (and our smoothing window  
133 great enough) to simply use linear interpolation. The total integration period for the wave  
134 tracing was 48 hours.

### 135 **3. Results**

136 As discussed in Harden *et al.* (2016), the vertical sections of velocity and hydrography  
137 at the Kögur site show the signatures of both the NIJ and the Separated EGC. However, the  
138 two features are merged to some degree in the mean (Figure 2). The NIJ is on the upper  
139 Iceland slope and is characterized by a mid-depth intensified flow carrying the coldest,  
140 densest overflow water banked up on the slope. The Separated EGC is farther offshore;  
141 its key features are a surface intensification and the transport of warmer, saltier overflow  
142 water at approximately 300 m. Inshore of both these currents, on the Iceland shelf, is the  
143 poleward flowing NIIC (see also Figure 1).

144 The two overflow currents are merged in the mean largely due to the high degree  
145 of variability on weekly timescales. The depth-integrated, along-stream velocity exhibits  
146 constant pulsing through this portion of the strait (Figure 3a). The period of the pulsing  
147 in the vicinity of the NIJ is concentrated at sub-8-day periods with a maximum average  
148 energy at 3.6 days (Figure 4). Farther offshore, near the Separated EGC, we also see  
149 such short-period pulses in addition to more consistent longer-period variability (Figure  
150 3a). The lower frequency signals were described by Harden *et al.* (2016) and attributed in  
151 part to the time-varying upstream bifurcation of the EGC. Here we focus on the higher-  
152 frequency, sub-8-day variability. To facilitate this we used an 8-day butterworth filter.<sup>1</sup>

153 The variance ellipses of this high-frequency variability for each mooring are useful  
154 for characterizing different regimes across the array (Figure 5). In the NIIC (KGA 1), the

---

<sup>1</sup>Different period filters were implemented, ranging in length from 4 days to 30 days, but the 8-day filter was most effective in isolating the peak high-frequency energy.

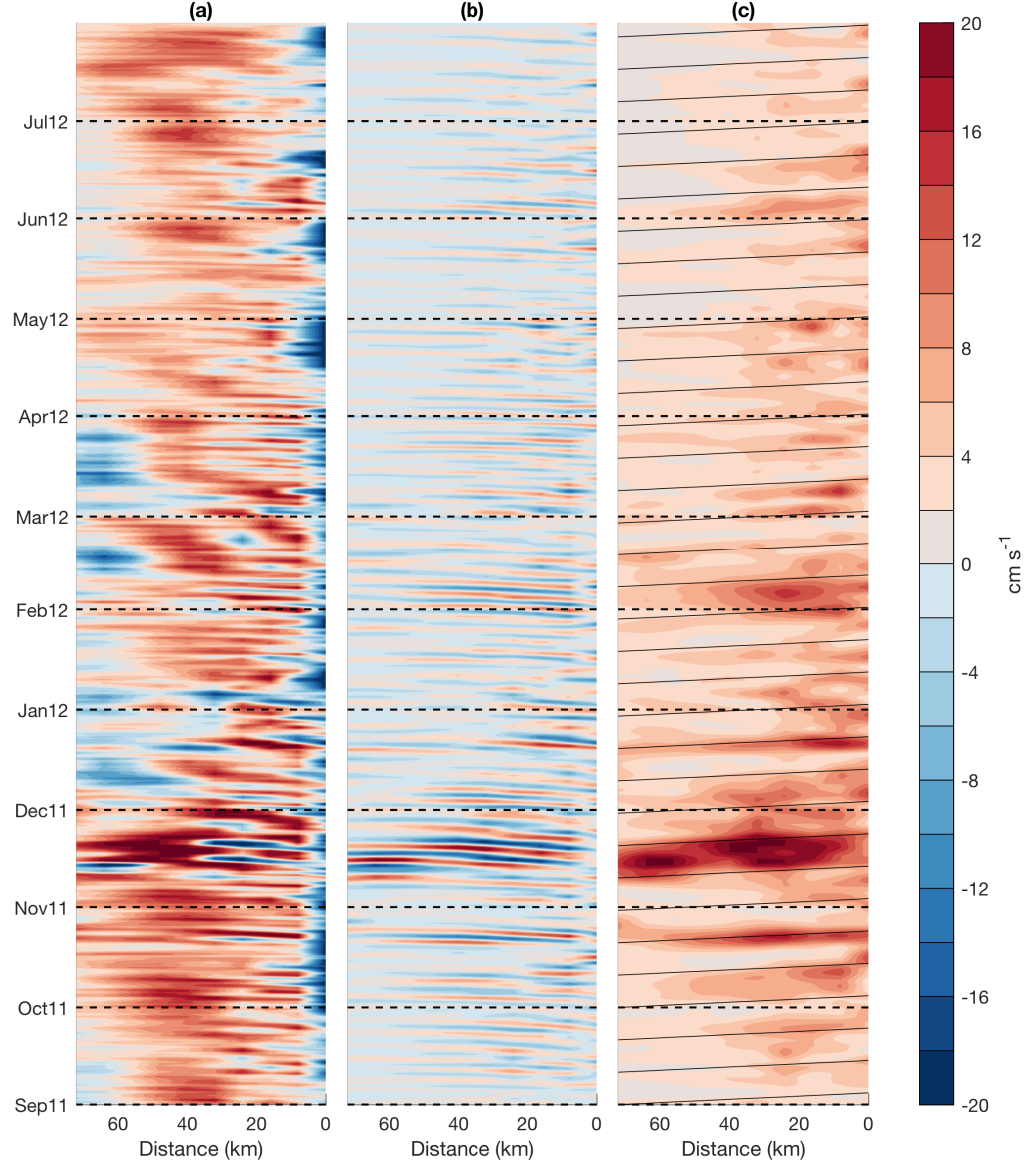


Figure 3: Hovmöller plots from the gridded mooring data of a) the depth-mean along-stream velocity (below 100 m, same for all plots); b) the 8-day high-passed, depth-mean component of velocity in the direction of the major axis of the local variance ellipse; and c) the wavelet amplitude at a 4-day period for the depth-mean velocity. Iceland is to the right of each panel as in Figure 2. The wavelet analysis uses the jLab toolbox (Lilly, 2017) with standard Morlet wavelets with  $\gamma=3$  and  $\beta=2$ . The sloped, black guidelines in panel c are angled at the theoretical group velocity for the measured topographic Rossby waves (see text for details).

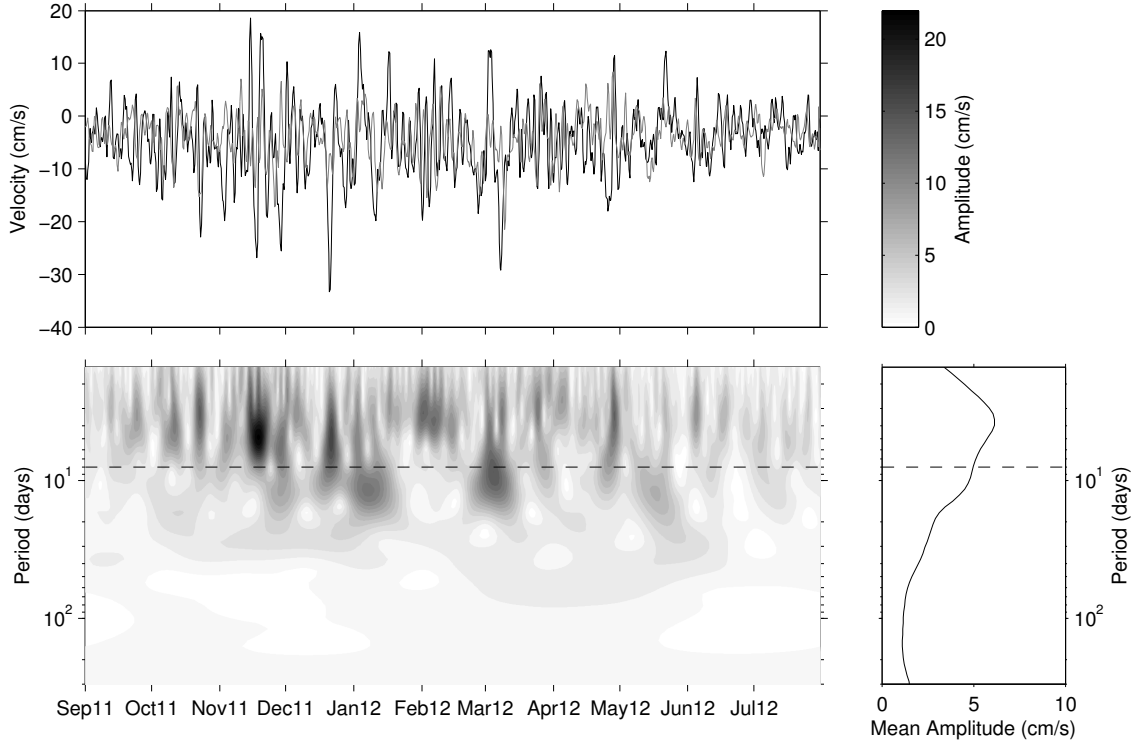


Figure 4: Top: Depth-averaged along-stream (black) and cross-stream (grey) components of velocity for the grid point closest to mooring KGA 3. Bottom left: Wavelet spectrum of the depth-averaged velocity using Morlet wavelets (Lilly, 2017). The color scale for this plot is at the top right. Bottom right: Mean wavelet amplitude for the length of the deployment. The dashed line in the bottom panels indicates the 8-day cut-off period for the high-pass filter used in this study.

155 variance ellipse is elongated in the direction of the mean flow indicative of a current puls-  
 156 ing along its axis. By contrast, within the Separated EGC (KGA 6 and 7), the elongation of  
 157 the variance ellipses is perpendicular to the mean flow demonstrating that this current me-  
 158 anders. However, in the NIJ (KGA 2-4), the major axes of the variance ellipses are aligned  
 159 at an oblique angle to both the mean flow and the underlying bathymetry. KGA 5 appears  
 160 to be in a transition region between conditions in the NIJ and those in the Separated EGC.

#### 161 *a. Topographic Rossby Waves*

162 We resolved the sub-8-day depth-averaged flow in the gridded product along the major  
 163 axis of the variance ellipses at each offshore location. Particularly in the NIJ, the variability  
 164 along these axes have a sinusoidal form and are lagged between moorings such that the

165 pulses of current progress offshore in time (Figure 3b). This implies a downslope phase  
 166 propagation of this variability.

167 We argue that this is the signature of TRWs. These waves are supported by topo-  
 168 graphic  $\beta$  and result in transverse fluctuations that are often at an oblique angle to the  
 169 mean flow. TRWs are found in many slope regions of the worlds oceans (Garrett, 1979;  
 170 Louis *et al.*, 1982; Pickart and Watts, 1990). Key features of TRWs include wave vec-  
 171 tors (and hence phase velocities) that are perpendicular to the velocity variability, a group  
 172 velocity which is at an oblique angle to the phase velocity, and a tendency to be bottom-  
 173 trapped in regions of significant stratification.

174 Given that the phase propagation is perpendicular to the velocity variability, we de-  
 175 duce that the wave phase is progressing downslope at  $-9^\circ\text{T}$  (average from moorings KGA  
 176 2–4, see Figure 5). Following Pickart and Watts (1990), we then calculated the phase  
 177 speed over the range of moorings KGA 2–4 (where the wave signal is most pronounced)  
 178 using,

$$c_p = \frac{1}{T} \frac{360}{\bar{\phi}} \frac{\overline{\Delta S}}{\cos(\Delta)}$$

179 where  $T$  is the wave period ( $= 3.6$  days),  $\bar{\phi}$  is the average phase offset ( $= 48 \pm 3^\circ$ ),  
 180  $\overline{\Delta S}$  is the average instrument spacing ( $= 8.1 \pm 0.2$  km), and  $\Delta$  is the angle between the  
 181 mooring array and the direction of wave propagation ( $= 8 \pm 4^\circ$ ). The resulting phase  
 182 speed is  $17.3 \pm 0.8$  km day $^{-1}$  corresponding to a wavelength of  $62 \pm 3$  km. The error  
 183 estimates arise in equal contributions from uncertainties in  $\bar{\phi}$ ,  $\overline{\Delta S}$ , and  $\Delta$ .

184 As a consistency check that the observed fluctuations are in fact TRWs, we can em-  
 185 ploy the TRW dispersion relation for a uniformly stratified ocean neglecting planetary  $\beta$ .  
 186 Following Pedlosky (1979), this can be written as:

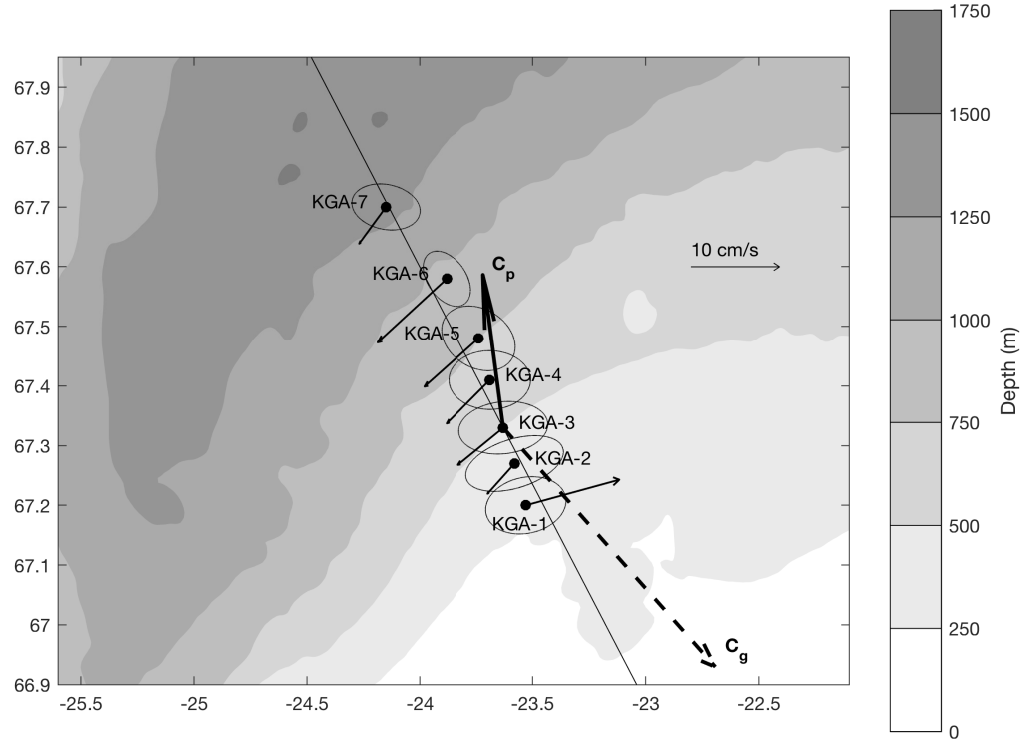


Figure 5: Aspects of the flow measured by the Kögur moorings (black circles). The thin vectors indicate the mean velocity averaged from 100 m to the depth of the ADCP at each mooring (see gray lines in Figure 2). Also shown are the 8-day high-passed variance ellipses for the same depth range. The thick black arrow ( $C_p$ ) denotes the direction of TRW phase propagation averaged over KGA 2-4 (plotted at KGA 3). The dashed black arrow shows the direction of TRW group velocity ( $C_g$ ). All vectors and variance ellipses are drawn to the same scale as indicated. The long black line is the mean downslope direction averaged between KGA 2-4. Bathymetry is from IBCAO v3.

$$T = \frac{2\pi \tanh(\frac{2\pi ND}{\lambda f})}{N\Gamma \sin(\theta)}$$

187 where  $T$  is the period of the wave,  $N$  is the average water column Brunt Väisälä  
188 frequency ( $= 3.3 \times 10^{-5}$ , averaged using the gridded data below 100 m),  $D$  is the depth

189 ( $= 500$  m),  $\lambda$  is the wavelength,  $f$  is the Coriolis parameter ( $= 1.35 \times 10^{-4}$ ),  $\Gamma$  is the  
190 bottom slope ( $= 0.016$ , from IBCAO v3), and  $\theta$  is the phase velocity direction relative to  
191 downslope.

192 We can test the predicted value of  $\theta$  against the observed value using our knowledge  
193 of the other variables. The predicted angle of  $29^\circ$  compares well with the measured value  
194 of  $24^\circ$  (from the average downslope angle between moorings KGA 2–4). There is of  
195 course uncertainty in the measured downslope angle depending on the region selected  
196 for the averaging. For example, if we expand the calculation of the downslope direction  
197 to encompass KGA 1–5, the measured  $\theta$  becomes  $33^\circ$ , which still agrees well with the  
198 predicted value. In addition, the bottom-trapping scale ( $= f/Nk$ ) is much greater than  
199 1000 m, in agreement with the observed velocities which are largely barotropic.

200 All of this supports our assertion that the dominant high-frequency variability in the  
201 NIJ is due to TRWs. The obvious question is, where and how are these waves being  
202 generated? Using the dispersion relation we can calculate the group velocity. For the  
203 observed parameters, we find this to be  $36 \text{ km day}^{-1}$  directed almost directly up-slope at  
204 the array site ( $138^\circ\text{T}$ , see Figure 5). This implies that the energy source lies offshore.  
205 We can corroborate this onshore propagation of energy observationally by considering the  
206 wavelet amplitude for the 4-day signal at each mooring site. The Hovmöller plot of this  
207 shows clear occurrences of onshore energy propagation that are in line with the predicted  
208 group velocity (Figure 3c).

## 209 *b. Wave Tracing and TRW Formation Mechanisms*

210 In order to shed light on the source of the TRWs, we implemented the inverse wave  
211 tracing model described in Section 2. In particular, we calculated the wave paths back-  
212 wards in time from moorings KGA 2–5. For each mooring, the model was initialized  
213 with the local wavenumber (assuming constant phase velocity and wave period). Since  
214 KGA 5 only marginally displayed TRW behavior, the results from that mooring should  
215 be considered less robust. The calculated paths indicate that the waves originate offshore

216 of the moorings in the vicinity of the deep Blosseville Basin (Figure 6). While the traces  
217 diverge somewhat going offshore, it is clear that they do not deflect significantly upstream  
218 or downstream. In other words, the energy is not propagating along the Iceland continental  
219 slope.

220 TRWs are a ubiquitous feature in the middle Atlantic Bight between Cape Hatteras,  
221 NC and the Grand Banks (Louis *et al.*, 1982; Johns and Watts, 1986; Pickart and Watts,  
222 1990). The source of the waves appears to be the Gulf Stream. Both Hogg (1981) and  
223 Schultz (1987) argued that TRWs observed along the US continental slope emanated from  
224 large amplitude Gulf Stream meanders offshore. Louis *et al.* (1982) made the case that  
225 bursts of TRWs measured south of Nova Scotia resulted from Gulf Stream eddy formation.  
226 Pickart (1995) demonstrated that the TRWs observed near Cape Hatteras were forced by  
227 meanders of the Gulf Stream as it flowed over a bend in topography farther to the east.

228 In light of these studies, it is natural to suspect that the TRWs measured at the Kögur  
229 array site are generated by the Separated EGC. This current is energetic, and, as noted  
230 above, is subject to significant meandering (akin to the Gulf Stream). The wave tracing  
231 indicates that the energy emanates from the Blosseville Basin where the Separated EGC  
232 resides. Additionally, there is evidence that times of strong TRW activity on the upper  
233 slope are often preceded slightly by increases in meander energy offshore (Figure 3). The  
234 high-energy event in November is one example of this, but there are additional instances  
235 in late October, late December, and early March.

236 Another possible trigger for the waves is the intermittent aspiration of deeper waters  
237 towards the Denmark Strait Sill. Harden *et al.* (2016) demonstrated that 0.6 Sv of the  
238 overflow transport approaching the sill does so from below sill depth. Pulsing of this  
239 aspirated component of the flow across the isobaths could initiate topographic wave activ-  
240 ity. Regardless of the mechanism, the presence of TRWs raises the question of whether  
241 they are present along the entire Iceland slope or whether they are unique to our sampling  
242 region. To address this we examined the velocity data from a mooring deployed approxi-

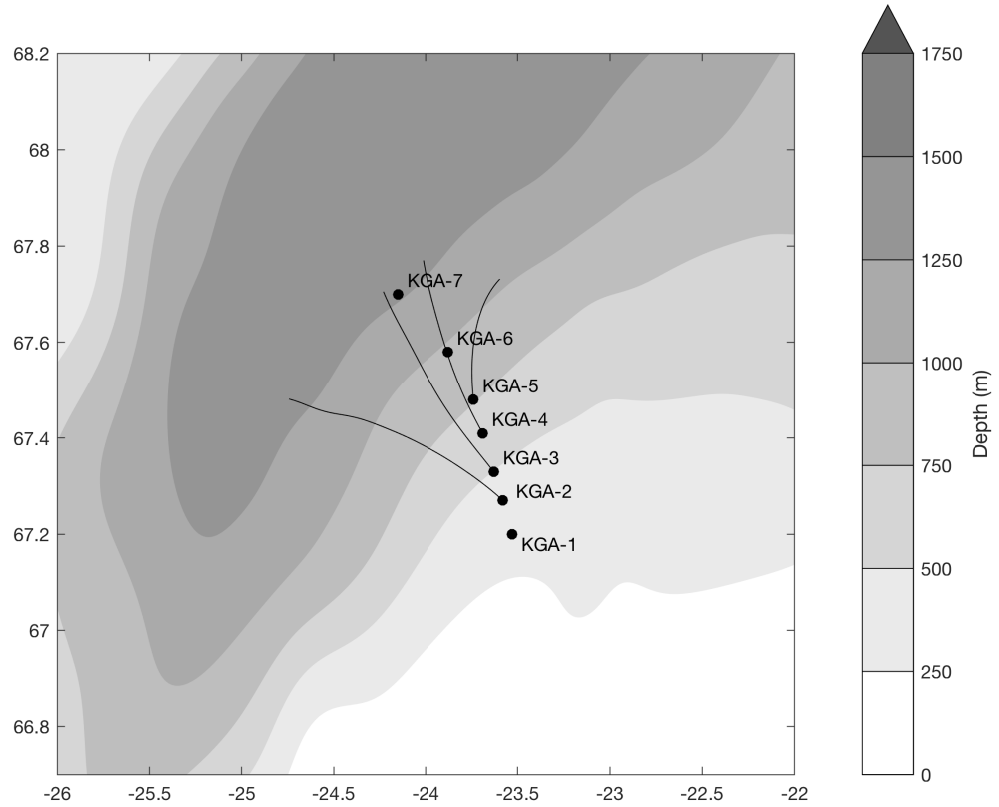


Figure 6: Paths of the Topographic Rossby Waves (thin lines) computed using the inverse wave tracing model for moorings KGA 2-5. Wave traces are truncated as they pass the 1500 m isobath. The bathymetry is from IBCAO v3 smoothed over 60 km (see text for details).



243 mately 200 km upstream on the Iceland slope near the Kolbeinsey ridge from 2007–2008  
244 (Jónsson and Valdimarsson, 2012). The depth-mean velocity showed very little energy  
245 in the 4-day period, at odds with the large TRW signal found at this period at the Kögur  
246 array. Notably, the upstream mooring site is quite far from the Separated EGC (Figure 1)  
247 and hence lacks that as an energy source.

## 248 **4. Summary and Discussion**

249 We have documented the existence of energetic Topographic Rossby Waves (TRWs)  
250 within the North Icelandic Jet (NIJ) using observations from the densely-instrumented  
251 Kögur Array located approximately 200 km upstream of the Denmark Strait Sill. The  
252 mean period of the waves is 3.6 days, the wavelength is  $62 \pm 3$  km, and the phase velocity  
253 is  $17.3 \pm 0.8$  km day<sup>-1</sup> directed downslope ( $-9^\circ\text{T}$ ). Using the TRW dispersion relation,  
254 we corroborated our observed direction of phase propagation relative to the downslope  
255 direction ( $24^\circ$ ) with the theoretical value ( $29^\circ$ ). We further calculated that the wave energy  
256 is progressing up-slope ( $138^\circ\text{T}$ ) at  $36$  km day<sup>-1</sup>, in agreement with our observational  
257 data. It is likely that the energy in the TRWs emanates locally near the mooring site,  
258 either through the meandering of the offshore Separated East Greenland Current (EGC),  
259 or through pulses of cross-bathymetric flow due to the aspiration of deep overflow water  
260 as it approaches Denmark Strait.

261 Notably, our data imply that the dominant high-frequency variability at the Kögur site  
262 does not originate from the Denmark Strait, nor does it propagate towards the sill. This is  
263 perhaps surprising in light of the fact that fluctuations of the dense overflow water at the sill  
264 occur on similar short timescales (Jochumsen *et al.*, 2017). It suggests that the mesoscale  
265 features at the sill (boluses and pulses), diagnosed observationally by Appen *et al.* (2017)  
266 and in a model framework by Almansi *et al.* (2017), are not triggered, nor directly trig-  
267 ger, the TRWs on the Iceland Slope. However, the likelihood of a connection between  
268 these features is still high given the geographic proximity and similarity in timescales, but

269 is presumably mediated by another process. The Denmark Strait overflow is believed to  
270 be subject to hydraulic control (Whitehead, 1998; Nikolopoulos *et al.*, 2003), and conse-  
271 quently, information should be transferred between upstream and sill variability, likely as  
272 Kelvin waves. The existence of any such connection and the impact on both the sill and  
273 NIJ variability requires more careful investigation and is the subject of an on-going study.

274 Finally, one also needs to consider where the energy in the TRWs ends up and what  
275 impact it might have on the dynamics of the circulation inshore of the Iceland slope. The  
276 energy likely cascades into the North Icelandic Irminger Current (NIIC) where it dissi-  
277 pates, leading to enhanced mixing. It might also alter the stability of NIIC, which brings  
278 warm subtropical water into the Nordic Seas. (Våge *et al.*, 2011) hypothesize that the  
279 offshore flux of this warm water associated with the disintegration of the NIIC is tied to  
280 the overturning loop that forms the NIJ. Notably, eddies of NIIC water are found both in  
281 the Blosseville Basin (Jónsson and Valdimarsson, 2012) and farther north in the Iceland  
282 Sea (Våge *et al.*, 2011). It is intriguing to think that the TRWs described here could play  
283 a role in this aspect of the NIIC.

284 *Acknowledgments.* We would like to thank the crew and technicians aboard the R/V  
285 Knorr and RSS James Clark Ross for the deployment and recovery of the Kögur moorings.  
286 This work was supported by National Science Foundation grants OCE-0959381 (BH and  
287 RP) and OCE-1558742 (RP).

288

## 289 REFERENCES

290 Almansi, M., T. W. N. Haine, R. S. Pickart, M. G. Magaldi, R. Gelderloos, and D. Mas-  
291 tropole. 2018/01/05 2017. High-frequency variability in the circulation and hydrog-  
292 raphy of the denmark strait overflow from a high-resolution numerical model. Journal

293 of Physical Oceanography, 47(12), 2999–3013. doi: 10.1175/JPO-D-17-0129.1. URL  
294 <https://doi.org/10.1175/JPO-D-17-0129.1>.

295 Appen, W.-J. v., D. Mastropole, R. S. Pickart, H. Valdimarsson, S. Jónsson, and J. B.  
296 Girton. 2017/08/03 2017. On the nature of the mesoscale variability in denmark strait.  
297 Journal of Physical Oceanography, 47(3), 567–582. doi: 10.1175/JPO-D-16-0127.1.  
298 URL <https://doi.org/10.1175/JPO-D-16-0127.1>.

299 Behrens, E., K. Våge, B. Harden, A. Biastoch, and C. W. Böning. 2017.  
300 Composition and variability of the denmark strait overflow water in a high-  
301 resolution numerical model hindcast simulation. Journal of Geophysical Re-  
302 search: Oceans, 122(4), 2830–2846. doi: 10.1002/2016JC012158. URL  
303 <http://dx.doi.org/10.1002/2016JC012158>.

304 Bruce, J. 1995. Eddies southwest of the Denmark Strait.  
305 Deep Sea Research Part I: Oceanographic Research Papers, 42  
306 (1), 13–29. doi: 10.1016/0967-0637(94)00040-Y. URL  
307 <http://www.ingentaconnect.com/content/els/09670637/1995/00000042/000>

308 Cooper, L. H. N. 1955. Deep water movements in the north atlantic as a link between  
309 climatic changes around iceland and biological productivity of the english channel and  
310 celtic sea. Journal of Marine Research, pages 347–362.

311 Dickson, R. R. and J. Brown. 1994. The production of North At-  
312 lantic Deep Water: Sources, rates, and pathways. J. Geophys. Res., 99  
313 (C6), 12319–12341. ISSN 0148-0227. doi: 10.1029/94JC00530. URL  
314 <http://dx.doi.org/10.1029/94JC00530>.

315 Garrett, C. 2017/08/08 1979. Topographic rossby waves off east australia: Iden-  
316 tification and role in shelf circulation. Journal of Physical Oceanography, 9

317 (2), 244–253. doi: 10.1175/1520-0485(1979)009;0244:TRW0EA;2.0.CO;2. URL  
 318 [https://doi.org/10.1175/1520-0485\(1979\)009<0244:TRW0EA>2.0.CO;2](https://doi.org/10.1175/1520-0485(1979)009<0244:TRW0EA>2.0.CO;2).

319 Harden, B. E., R. S. Pickart, H. Valdimarsson, K. Våge, L. de Steur, C. Richards,  
 320 F. Bahr, D. Torres, E. Børve, S. Jónsson, A. Macrander, S. Østerhus, L. Håvik, and  
 321 T. Hattermann. 6 2016. Upstream sources of the denmark strait overflow: Observations  
 322 from a high-resolution mooring array. *Deep Sea Research Part I: Oceanographic*  
 323 *Research Papers*, 112, 94–112. doi: <https://doi.org/10.1016/j.dsr.2016.02.007>. URL  
 324 <http://www.sciencedirect.com/science/article/pii/S0967063715301266>.

325 Håvik, L., K. Våge, R. S. Pickart, B. Harden, W. J. von Appen, S. Jónsson, and S. Øster-  
 326 hus. 2017/08/30 2017. Structure and variability of the shelfbreak east greenland current  
 327 north of denmark strait. *Journal of Physical Oceanography*. doi: 10.1175/JPO-D-17-  
 328 0062.1. URL <https://doi.org/10.1175/JPO-D-17-0062.1>.

329 Hogg, N. G. 1981. Topographic waves along 70°w on the continental rise. *Journal of*  
 330 *Marine Research*, 39, 627–649.

331 Jakobsson, M., L. Mayer, B. Coakley, J. A. Dowdeswell, S. Forbes, B. Fridman, H. Hod-  
 332 nesdal, R. Noormets, R. Pedersen, M. Rebesco, H. W. Schenke, Y. Zarayskaya, D. Ac-  
 333 cettella, A. Armstrong, R. M. Anderson, P. Bienhoff, A. Camerlenghi, I. Church,  
 334 M. Edwards, J. V. Gardner, J. K. Hall, B. Hell, O. Hestvik, Y. Kristoffersen, C. Mar-  
 335 cussen, R. Mohammad, D. Mosher, S. V. Nghiem, M. T. Pedrosa, P. G. Travaglini, and  
 336 P. Weatherall. 2012. The international bathymetric chart of the arctic ocean (ibcao) ver-  
 337 sion 3.0. *Geophysical Research Letters*, 39(12), n/a–n/a. doi: 10.1029/2012GL052219.  
 338 URL <http://dx.doi.org/10.1029/2012GL052219>.

339 Jochumsen, K., M. Moritz, N. Nunes, D. Quadfasel, K. M. H. Larsen,  
 340 B. Hansen, H. Valdimarsson, and S. Jonsson. 2017. Revised trans-  
 341 port estimates of the denmark strait overflow. *Journal of Geophysical Re-*

342 search: *Oceans*, 122(4), 3434–3450. doi: 10.1002/2017JC012803. URL  
 343 <http://dx.doi.org/10.1002/2017JC012803>.

344 Johns, W. E. and D. R. Watts. 1986. Time scales and structure of topo-  
 345 graphic rossby waves and meanders in the deep gulf stream. *Journal of Ma-*  
 346 *rine Research*, 44(2), 267–290. doi: 10.1357/002224086788405356. URL  
 347 <http://www.ingentaconnect.com/content/jmr/jmr/1986/00000044/00000002>

348 Jonsson, S. and H. Valdimarsson. February 2004. A new path for the denmark strait over-  
 349 flow water from the iceland sea to denmark strait. *Geophys. Res. Lett.*, 31(3), L03305–.  
 350 ISSN 0094-8276. URL <http://dx.doi.org/10.1029/2003GL019214>.

351 Jónsson, S. and H. Valdimarsson. 06 2012. Hydrography and circulation over the southern  
 352 part of the Kolbeinsey Ridge. *ICES Journal of Marine Science: Journal du Conseil*.

353 Käse, R. H., J. B. Girton, and T. B. Sanford. 2003. Structure and variabil-  
 354 ity of the Denmark Strait Overflow: Model and observations. *Journal of Geo-*  
 355 *physical Research: Oceans*, 108(C6), 3181. doi: 10.1029/2002JC001548. URL  
 356 <http://dx.doi.org/10.1029/2002JC001548>.

357 Lilly, J. M. 2017. jlab: A data analysis package for matlab, v 1.6.3.

358 Louis, J. P., B. D. Petrie, and P. C. Smith. 2017/08/08 1982. Ob-  
 359 servations of topographic rossby waves on the continental margin  
 360 off nova scotia. *Journal of Physical Oceanography*, 12(1), 47–55.  
 361 doi: 10.1175/1520-0485(1982)012<0047:OOTRWO>2.0.CO;2. URL  
 362 [https://doi.org/10.1175/1520-0485\(1982\)012<0047:OOTRWO>2.0.CO;2](https://doi.org/10.1175/1520-0485(1982)012<0047:OOTRWO>2.0.CO;2).

363 Mastropole, D., R. S. Pickart, H. Valdimarsson, K. Våge, K. Jochumsen, and J. Gir-  
 364 ton. 2017. On the hydrography of denmark strait. *Journal of Geophysi-*  
 365 *cal Research: Oceans*, 122(1), 306–321. doi: 10.1002/2016JC012007. URL  
 366 <http://dx.doi.org/10.1002/2016JC012007>.

- 367 Mauritzen, C. 1996. Production of dense overflow waters feeding the North  
368 Atlantic across the Greenland-Scotland Ridge. Part 1: Evidence for a re-  
369 vised circulation scheme. Deep Sea Research Part I: Oceanographic Re-  
370 search Papers, 43(6), 769–806. doi: 10.1016/0967-0637(96)00037-4. URL  
371 <http://www.sciencedirect.com/science/article/pii/0967063796000374>.
- 372 Meinen, C., E. Fields, R. S. Pickart, and D. R. Watts. 1993. Ray tracing on topographic  
373 rossby waves. Technical Report 93-1, University of Rhode Island.
- 374 Nikolopoulos, A., K. Borenäs, R. Hietala, and P. Lundberg. 2003. Hy-  
375 draulic estimates of Denmark Strait overflow. Journal of Geophysical Re-  
376 search: Oceans, 108(C3), 3095. doi: 10.1029/2001JC001283. URL  
377 <http://dx.doi.org/10.1029/2001JC001283>.
- 378 Pedlosky, J. 1979. *Geophysical Fluid Dynamics*. Springer US. doi: 10.1007/978-1-4684-  
379 0071-7.
- 380 Pickart, R. S. 1995. Gulf stream-generated topographic rossby  
381 waves. Journal of Physical Oceanography, 25(4), 574–586.  
382 doi: 10.1175/1520-0485(1995)025<0574:GSTRW>2.0.CO;2. URL  
383 [https://doi.org/10.1175/1520-0485\(1995\)025<0574:GSTRW>2.0.CO;2](https://doi.org/10.1175/1520-0485(1995)025<0574:GSTRW>2.0.CO;2).
- 384 Pickart, R. S. and D. R. Watts. 1990. Deep western boundary current vari-  
385 ability at cape hatteras. Journal of Marine Research, 48(4), 765–791. URL  
386 <http://www.ingentaconnect.com/content/jmr/jmr/1990/00000048/00000004>
- 387 Pickart, R. S., M. A. Spall, D. J. Torres, K. Våge, H. Valdimarsson,  
388 C. Nobre, G. W. K. Moore, S. Jonsson, and D. Mastropole. 2017.  
389 The north icelandic jet and its relationship to the north icelandic  
390 irmingier current. Journal of Marine Research, 75(5), 605–639. URL  
391 <http://www.ingentaconnect.com/content/jmr/jmr/2017/00000075/00000005>

- 392 Rudels, B., E. Fahrbach, J. Meincke, G. Budéus, and P. Eriksson. 2002. The East Green-  
393 land Current and its contribution to the Denmark Strait overflow. *ICES Journal of Ma-  
394 rine Science: Journal du Conseil*, 59, 1133–1154. doi: 10.1006/jmsc.2002.1284.
- 395 Schultz, R. J., 1987. Structure and propagation of topographic rossby waves northeast of  
396 cape hatteras, north carolina. Master's thesis, Marine Science Program, University of  
397 North Carolina.
- 398 Smith, P. C. May 1976. Baroclinic Instability in the Denmark  
399 Strait Overflow. *J. Phys. Oceanogr.*, 6(3), 355–371. ISSN 0022-  
400 3670. doi: 10.1175/1520-0485(1976)006<0355:BIITDS>2.0.CO;2. URL  
401 [http://dx.doi.org/10.1175/1520-0485\(1976\)006<0355:BIITDS>2.0.CO;2](http://dx.doi.org/10.1175/1520-0485(1976)006<0355:BIITDS>2.0.CO;2).
- 402 Strass, V. H., E. Fahrbach, U. Schauer, and L. Sellmann. 1993. Formation of Den-  
403 mark Strait overflow water by mixing in the East Greenland Current. *Journal of Geo-  
404 physical Research: Oceans*, 98(C4), 6907–6919. doi: 10.1029/92JC02732. URL  
405 <http://dx.doi.org/10.1029/92JC02732>.
- 406 Våge, K., R. S. Pickart, M. A. Spall, H. Valdimarsson, S. Jónsson, D. J. Torres, S. Øster-  
407 hus, and T. Eldevik. 2011. Significant role of the North Icelandic Jet in the formation  
408 of Denmark Strait overflow water. *Nature Geosci*, 4(10), 723–727. ISSN 1752-0894.  
409 doi: 10.1038/ngeo1234. URL <http://dx.doi.org/10.1038/ngeo1234>.
- 410 Våge, K., R. S. Pickart, M. A. Spall, G. W. K. Moore, H. Valdimarsson, D. J.  
411 Torres, S. Y. Erofeeva, and J. E. Ø. Nilsen. 2013. Revised circulation  
412 scheme north of the Denmark Strait. *Deep Sea Research Part I: Oceano-  
413 graphic Research Papers*, 79(0), 20–39. doi: 10.1016/j.dsr.2013.05.007. URL  
414 <http://www.sciencedirect.com/science/article/pii/S0967063713001040>.
- 415 Våge, K., G. W. K. Moore, S. Jónsson, and H. Valdimarsson. 2015. Water  
416 mass transformation in the Iceland Sea. *Deep Sea Research Part I: Oceano-*

417 graphic Research Papers, *101*(0), 98–109. doi: 10.1016/j.dsr.2015.04.001. URL  
418 <http://www.sciencedirect.com/science/article/pii/S0967063715000680>.

419 Whitehead, J. A. 1998. Topographic control of oceanic flows in deep passages and  
420 straits. *Reviews of Geophysics*, *36*(3), 423–440. doi: 10.1029/98RG01014. URL  
421 <http://dx.doi.org/10.1029/98RG01014>.